December 1960 and January, February, March, July, and August 1961, respectively. The dark areas correspond to a positive energy balance, that is, an excess of incoming radiation over the outgoing. The light areas indicate regions of negative balance. In these figures, the darkest shade (for example, southwestern United States in July) has a value of $> + 1.75 \times 10^5$ ergs cm^{-2} sec^{-1}, while the lightest shade (for example, 40°N to 50°N belt in December) corresponds to $< -1.65 \times 10^5$ ergs cm^{-2} sec^{-1}. The intermediate values of the energy balance are plotted, in steps of about 0.5×10^5 ergs cm^{-2} sec^{-1}, as seven gradations of the shading level.

The two triangular regions comprising parts of South America and Siberia have been left blank because data from Tiros are not available in those regions. Also the several other 10° by 10° grids left blank in March and July are due to nonavailability of data from Tiros for these regions.

A preliminary examination of these figures reveals several interesting features.

1) In December and January, the regions of maximum positive energy input are located in the latitudinal belts of 20°S to 50°S, while in July and August it is the 10°N to 40°N belt which has a high excess of energy. The evolution of this phenomenon is revealed by the charts for February and March.

2) The geographical distribution of the energy balance appears to be such that the desert areas of Africa, Australia, the Middle East, and southwestern United States show extreme positive energy inputs in the local summer.

3) The effect of the monsoon over India is noticeable in comparing the charts for March and August 1961. The net energy input over India is lower in August than in March, presumably because of the heavy monsoon cloud cover, although if it were not for the monsoon, one would expect a very high excess of energy in the summer month of August.

4) In the Northern Hemisphere, the region of the western Pacific appears to show a relative deficit in energy during all the 6 months. This area is well known for strong cyclogenic activity. As in the case of the monsoon, the high cloudiness produced by the cyclogenesis probably accounts for the observed low input in energy.

A detailed analysis of these charts, in conjunction with the actually observed global distribution of the weather patterns for the respective months, may provide a better understanding of the role played by the energy balance of the atmosphere in the evolution of weather systems.

S. I. RASOOL
Goddard Institute for Space Studies, National Aeronautics and Space Administration, New York,
and *Department of Meteorology, New York University, New York*

References and Notes

1. G. C. Simpson, *Mem. Roy. Meteorol. Soc.* **3**, No. 23, 53 (1929).
2. G. H. Houghton, *J. Meteorol.* **11**, (1954).
3. J. London, "A study of the atmospheric heat balance," *Final Report*, Contract No. AF 19 (122)-165, Research Division, College of Engineering, New York University, New York, 1957.
4. F. A. Budyko, Jr., *The Heat Balance of the Earth's Surface*. Translated from the Russian edition by Nina A. Stepanova (U.S. Weather Bureau, Washington, D.C., 1958).
5. W. R. Bandeen, R. A. Hanel, J. Licht, R. A. Stampfl, W. G. Stroud, *J. Geophys. Res.* **65**, 3165 (1961).
6. W. Nordberg, W. R. Bandeen, B. J. Conrath, V. Kinde, I. Persano, *J. Atm. Sci.* **19**, 20 (1962).
7. A. Arking, *Science*, this issue.
8. D. G. Wark, G. Yamamoto, J. H. Lienesch, "Methods of estimating infrared flux and surface temperature from meteorological satellites," *J. Atmospheric Sci.* **19**, 369 (1962).
9. C. Prabhakara and S. I. Rasool, in *Proceedings of the 1st International Symposium on Rocket and Satellite Meteorology*, H. Wexler and J. E. Caskey, Jr., Eds. (North-Holland, Amsterdam, 1963).
10. I thank J. London, R. M. Goody, J. Charney, and R. Jastrow for many illuminating discussions, and Conrad Hipkins who computed and plotted these data on an IBM 7094 and SC 4020.

3 January 1964

Latitudinal Distribution of Cloud Cover from Tiros III Photographs

Abstract. *Television pictures from the Tiros III satellite have been analyzed on a computer to give the latitudinal distribution of cloud cover during the summer of 1961. The results, which will be useful in studying the heat balance of the atmosphere and in the determination of vertical motion, show good agreement with the long-term average cloudiness derived from data accumulated during 50 years of ground observations.*

The global distribution of cloud cover is now being investigated by the analysis of photographs from Tiros meteorological satellites. The aim of this cloud-cover study is to derive basic information on the radiation energy balance of the atmosphere, and on the vertical atmospheric motions which are revealed by the existence of clouds. The type of information yielded by this analysis is important for studies of climate and for investigations of the general circulation of the atmosphere.

The energy input which sets the atmosphere in motion is given by the difference between the incoming solar energy, consisting of radiation primarily in the visible part of the spectrum, and the outgoing energy, consisting of radiation from the earth and the atmosphere in the far infrared part of the spectrum. The main control over the incoming solar radiation is provided by clouds, which can reflect up to 80 percent of the incident visible radiation, depending upon their thickness and type. Reflection by the atmosphere and the underlying surface is much less; it is about 8 to 10 percent for the atmosphere, from 3 to 20 percent for most terrains, and, in general, only a few percent for large bodies of water. Calculations of the available solar energy are thus strongly dependent on knowledge of the cloud-cover distribution.

The most important factors which govern the distribution of the outgoing infrared radiation are the ground temperatures, the amount of water vapor in the atmosphere, and particularly the extent and height of the clouds.

It is thus seen that the distribution of cloudiness plays an important role in the determination of both the inflow and the outflow of energy through the earth's atmosphere. Thus far, the distribution of clouds—amount, types, and approximate heights—have all been taken from ground-based observations. Satellite observations enable us to obtain extensive cloud-cover data on a global scale in a relatively short period of time.

Each Tiros satellite contains two television camera systems which photograph the cloud cover. Some satellites (Tiros II, III, IV, and VII) contain, in addition, radiometers to measure emitted infrared radiation and reflected visible radiation from the earth, atmosphere, and clouds. The data from the visible and infrared radiometers would ordinarily be sufficient for deriving the energy balance, but only on Tiros VII did the visible radiometer channel work successfully. From the cloud-cover distribution, however, one can estimate the reflected radiation in the visible

spectrum and hence, the incoming solar radiation.

Use of the radiation data in determining the energy balance is discussed in a simultaneous publication by Rasool (*1*) in which references are made to other studies of the radiation data. Although the cloud-cover pictures have been used extensively for their synoptic value in the detection and tracking of storms and in present methods of weather forecasting, the analysis of the pictures to obtain statistical data on cloud cover, for application to energy-balance studies, has not been undertaken previously.

The analysis of the cloud-cover photographs was performed on an I.B.M. 7090 computer. Photographs are converted into digital form for insertion into the computer by dividing the photographic image into 250,000 picture elements to form a matrix of numbers, 500 by 500, each number representing the brightness of the corresponding picture element.

The main problem in the computer analysis of cloud pictures is the choice of a criterion, suitable for machine execution, which will distinguish clouds from clear areas. The brightness of the picture element should be a suitable criterion, since clouds will have higher reflectivities than clear areas except in snow-covered regions. The analysis is complicated by the fact that a cloud of given reflectivity can have a range of brightness depending on the relative angles of the sun and camera with respect to the surface appearing in the photograph, the structure and thickness of clouds, and the nature of the underlying terrain. In addition, there may be variations in the characteristics of the vidicon tube and associated electronics after the satellite is put into orbit. Nonetheless, it was found, by analysis of sample pictures, that the difference between the reflectivities of clouds and the underlying terrain is great enough so that it is possible to choose a brightness threshold which defines the cloud boundaries reliably (Fig. 1). It was further found that the threshold may vary considerably for pictures taken during different orbits, but it varies only slightly from picture to picture within an orbit. It was therefore necessary to determine a new threshold for each orbital sequence but not for each picture. This method does not distinguish between clouds and snow-covered terrain, and, furthermore, it may result in an overestimation of the cloudiness over regions of bright sand. However, only a very small fraction of the earth is covered by bright sand, and the season and regions covered by Tiros III rule out extensive snow-cover.

The location of cloudy and clear areas on a world map requires precise knowledge of the satellite's position and angular orientation at the time the photograph was taken (see Fig. 2). These data were supplied by the Meteorological Satellite Laboratory of the Weather Bureau and the Aeronomy and Meteorology Division of the Goddard Space Flight Center. The transformation from the image plane of the photograph into geographical coordinates is described by Frankel and Bristor (*2*) and by Mach (*3*).

There were 1447 Tiros III photographs available on video tape which were free from excessive noise and for which we were able to obtain all the data required for the transformation to geographical coordinates. All the pictures were processed on the 7090 computer and form the basis of the results presented here.

The end product of the computer analysis is a magnetic tape which contains a summary of every picture analyzed. A computer program interrogates this tape to provide the mean percentage of cloud cover over any specified geographic region during any interval of time. For the purposes of this introductory note, however, we will present only the latitudinal distribution of cloud cover for the summer of 1961.

The geographical distribution of the pictures is shown in Fig. 3; each asterisk on the map represents a single photograph. All were taken during day-

Gray levels 1-32

17

21

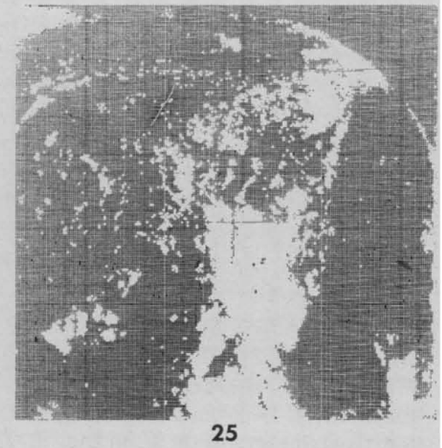

25

Fig. 1. Determination of brightness threshold of clouds (criteria for discriminating clouds from clear areas). A series of two-level images, in which intensities greater than a given threshold appear white and all others black, are produced for a number of thresholds, three of which are shown here. The number underneath each two-level image is the brightness level used as the threshold for the discrimination. The original full-tone image (gray levels 1–32) is compared with each two-level image to find the threshold which most closely reproduces the cloud boundaries reported by the human observer in the original image, in this case 21.

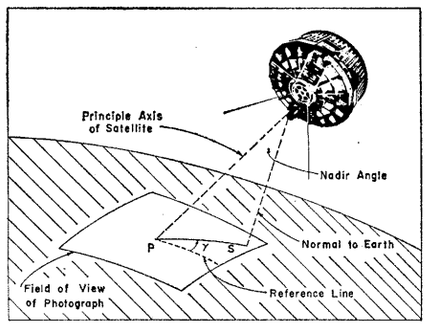

Fig. 2. Geometry of Tiros photography. The two television cameras point along the principal or spin axis of the satellite, which is fixed in space. The angle between the principal axis and the normal to the earth, the nadir angle, changes as the satellite orbits the earth. The intersection of the principal axis with the earth is called the principal point, denoted by P, and the point immediately below the satellite, called the subsatellite point, is denoted by S. As the satellite rotates, the image on the vidicon tube appears to rotate about the point P. The angle between PS and a fixed reference line on the vidicon tube defines the roll angle, γ, the value of which is required, in addition to the geographic positions of P and S, to transform from picture coordinates to geographic coordinates.

time between 12 July and 30 September 1961, between latitudes 60°S and 60°N. The number of pictures in the Southern Hemisphere is appreciably less than in the Northern Hemisphere and, consequently, errors due to statistical sampling will be greater for southern latitudes. There may also be some statistical bias in northern latitudes due to the sparseness of photographs over Asia.

The average latitudinal distribution of cloud cover is shown in Fig. 4 for the period 12 July to 30 September 1961. The solid horizontal bars give the mean percentage of earth area covered by clouds in intervals of 10° of latitude as determined from the Tiros III photographs. The vertical lines passing through the bars indicate the uncertainty estimated to arise in the threshold determination. Possible errors due to statistical sampling are not shown.

The results in Fig. 4 show that the cloud cover in middle latitudes is the same in the Northern and Southern Hemispheres. However, in tropical latitudes there is an asymmetry, with a local maximum of the cloud cover in the tropics centered at 10°N latitude. This is the average position of the "thermal equator" during the period 12 July to 30 September.

The broad features of the latitudinal distribution of cloud cover obtained from the Tiros photographs are consistent with the known pattern of the general circulation (*4*). Air rising at the thermal equator produces condensation and a relative maximum in the cloud cover, while on the average there is downward motion of cool, dry air at 30°C, which explains the relative minimum of cloudiness. The relationship between cloud-cover distribution and vertical air currents suggests that the Tiros cloud-cover statistics may have an important application in the determination of vertical motions in the atmosphere.

It is of considerable interest to compare the Tiros observations for the summer of 1961 with the climatological distributions of cloudiness found in the literature for the same season. Such distributions have been published by Haurwitz and Austin (*4*), Landsberg (*5*), and others for the globe; and, based on more extensive data, by Telegadas and London (*6*) for the Northern Hemisphere. The climatological results for the period July through September are shown by the dashed histogram in Fig. 4. The Northern Hemisphere data are taken from Telegadas and London (*6*); the Southern Hemisphere data are taken from Landsberg (*5*).

The Tiros results for 1961 are seen to be in good agreement with the long-term mean of cloud-cover distribution obtained from ground observations. The degree of correspondence between our

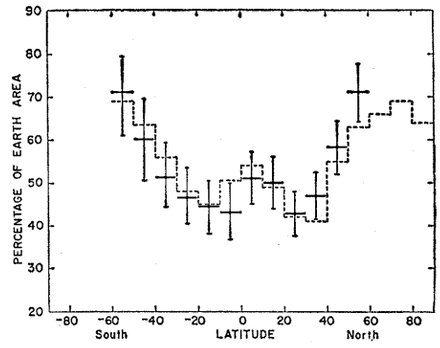

Fig. 4. The latitudinal distribution of cloud cover. The solid horizontal bars are the results derived from Tiros III photographs from 12 July to 30 September 1961. The vertical lines show the estimated uncertainty due to threshold determination. The dashed histogram represents the climatological mean cloud cover based upon ground observations, taken from Telegadas and London (*6*) for the Northern Hemisphere and from Landsberg (*5*) for the Southern Hemisphere

results and the ground-based data gives us confidence in this method of analysis of satellite photographs. The availability of more data from subsequent satellites will permit the determination of the geographical distribution of cloud cover over short intervals of time, for which no reliable information is now available. An increase in the density of observations, coupled with improvements in the techniques for picture analysis now being developed, should eventually lead to the use of cloud-cover pictures, auto-

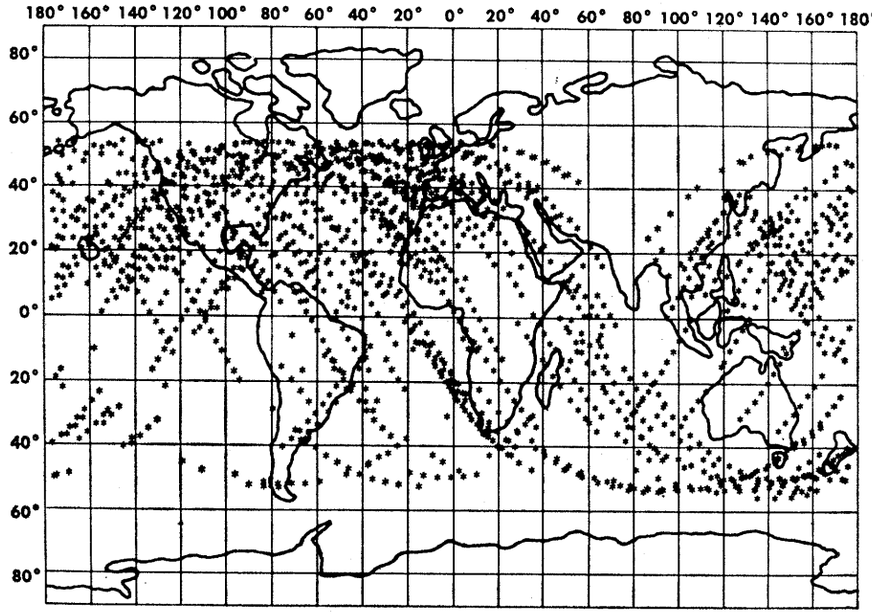

Fig. 3. The geographical distribution of the 1447 Tiros III pictures taken between 12 July and 30 September 1961 which were used in the analysis.

matically analyzed on a computer, to provide the cloud-cover distribution as a function of time for use in studies of atmospheric dynamics and long-term changes in climate.

ALBERT ARKING

Goddard Institute for Space Studies, National Aeronautics and Space Administration, New York 27, and *Department of Meteorology, New York University, New York*

References and Notes

1. S. I. Rasool, *Science*, this issue.
2. M. Frankel and C. L. Bristor, *Meteorological Satellite Laboratory Report No. 11*, Weather Bureau, U.S. Department of Commerce, 1962.
3. R. E. Mach, "Research on the processing of satellite photography by digital techniques," *Final Report, Contract AF 19(604) 8432*, International Business Machines Corp., 1962.
4. B. Haurwitz and J. M. Austin, *Climatology* (McGraw-Hill, New York, 1944).
5. H. Landsberg, "Climatology," *Handbook of Meteorology*, F. A. Berry, Jr., E. Bollay, N. R. Beers, Eds. (McGraw-Hill, New York, 1945), pp. 927–97.
6. K. Telegadas and J. London, "A physical model for the Northern Hemisphere for winter and summer," *Scientific Report No. 1*, Contract AF 19(122)-165, Research Division, College of Engineering, New York University, 1954.
7. We thank J. London of the University of Colorado for his suggestion of the original investigation, and for his detailed criticism of our results. We also thank J. Charney and R. Goody for helpful suggestions and Messrs. B. Kaufman and J. Borgelt and other members of the staff of Computer Applications, Inc., who developed the programs required for the reduction of the Tiros cloud-cover tapes.

3 January 1964

Fibrous Filters as Particle-Size Analyzers

Abstract. *A method was developed for characterizing radioactive aerosols by determining their distribution as a function of depth in fibrous filters under carefully controlled conditions. The method distinguishes the contributions of three major processes of filtration: diffusion, interception, and inertial impaction. For those experiments where diffusion is the controlling mechanism, particle sizes in the range of 50 to 500 Å thus determined compare favorably with those obtained from concentration and flow data and electron photomicrographs.*

The characterization of gas-borne particulate material, especially fission products which are released during a reactor accident, is necessary so that effective means may be developed for removing radioactivity from gas streams. We have developed a method for determining the sizes of radioactive particles, based on their interaction with fibers, using special techniques, considerably refined over the one first suggested by Sisefsky (*1*), for observing at various depths the distribution of radioactive particles in a filter.

The experimental arrangement was designed to facilitate separation of the fiber bed into discrete layers for radioassay after exposure to the aerosol. We chose fibers with a high degree of uniformity in order to facilitate theoretical analysis. Raw dacron-polyester staple fibers (99 percent were 11.3 ± 0.8 μ) 3.8 cm long were separted into a uniform web by means of a carding machine, and were then rolled between sheets of fine paper to give a product which has a fiber-volume fraction of 0.28 and the appearance and feel of filter paper. A number of disks of this material, 3.8 cm in diameter and 0.04 cm thick, were placed in series between metal washers, enclosed in a cylindrical Teflon holder, and provided with O-ring seals to give a compact filtering device. For testing, a radioactive aerosol containing Zn^{65} was produced by using a Tesla coil to generate a spark between two pieces of neutron-irradiated zinc foil placed approximately 2 mm apart. A stream of air passed over the electrodes and carried the aerosol through the system containing the filters. An electron micrograph of samples of the aerosol collected on a membrane filter showed that it consisted of particles whose diameter ranged from 20 to 350 Å (median diameter, 120 Å; geometric standard deviation, 2.0).

Experiments were conducted over a wide range, the linear flow rates varying from 0.2 to 44 cm/sec. The data were analyzed by means of graphs (Fig. 1) in which the log of the relative radioactivity collected per layer was plotted against depth in the filter. Each layer contained approximately 10^4 cm of fiber per square centimeter of filter area, evaluated from disk weights and the density of the fiber. The abscissa in Fig. 1 has been simplified to show filter depth in centimeters, but the very small nonuniformity of the filter pads has been accounted for in plotting the data. In the region of low flow where Brownian diffusion is the dominant process for particle transport to the fiber, filtration efficiency decreased with increasing velocity. In the high-flow region, where inertial impaction is the principal process for particle transport, the efficiency increased with increasing velocity. In the intermediate-flow region, the interception range, where geometrical considerations of particle size and fiber size are very important, the filtration efficiency is largely independent of

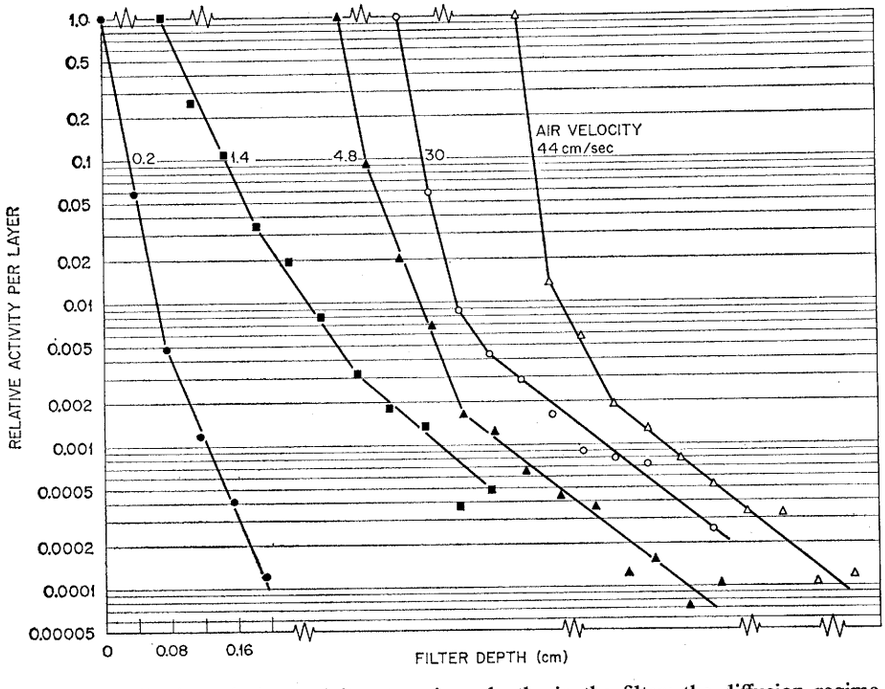

Fig. 1. Distribution of zinc activity at various depths in the filter; the diffusion regime at low air velocities can be recognized by the decrease of slope with increasing velocity.